Inorganic Chemistry

Article

pubs.acs.org/IC

Synthesis, Structure, and Electronic Properties of RuN_6 Dinuclear Ru-Hbpp Complexes

Stephan Roeser,[†] Mehmed Z. Ertem,[‡] Clyde Cady,[§] Rainer Lomoth,[§] Jordi Benet-Buchholz,[†] Leif Hammarström,[§] Biprajit Sarkar,[∥] Wolfgang Kaim,[∥] Christopher J. Cramer,*[,‡] and Antoni Llobet*[,†,⊥]

[†]Institute of Chemical Research of Catalonia (ICIQ), Av. Països Catalans 16, 43007 Tarragona, Spain

[‡]Department of Chemistry and Supercomputing Institute, University of Minnesota, 207 Pleasant Street SE, Minneapolis, Minnesota 55455, United States

[§]Department of Photochemistry and Molecular Science, Uppsala University, Box 523, 75120 Uppsala, Sweden

[∥]Institut für Anorganische Chemie, Universität Stuttgart, Pfaffenwaldring 55, D-70550 Stuttgart, Germany

[⊥]Departament de Química, Universitat Autònoma de Barcelona, Cerdanyola del Vallès, 08193 Barcelona, Spain

Supporting Information

ABSTRACT: A series of RuN_6 dinuclear Ru−Hbpp complexes (Hbpp is the dinucleating tetraaza ligand 3,5-bis(pyridyl)pyrazole) of general formula $\{[Ru^{II}(R^2\text{-trpy})(MeCN)]_2(\mu\text{-}R^1\text{-bpp})\}^{3+}$, $\mathbf{10}^{3+}$−$\mathbf{14}^{3+}$, (R^1 = H, Me, or NO_2. and R^2 = H, Me, MeO; see Scheme 1) has been prepared from their Cl^- or AcO^- bridged precursors. The complexes have been characterized by UV−vis, NMR, CV, and some by X-ray. Complexes $\mathbf{10}^{3+}$−$\mathbf{14}^{3+}$, $Ru_2^{II,II}$, were oxidized by 1 equiv in solution, leading to the mixed valence $Ru_2^{II,III}$ complexes $\mathbf{10}^{4+}$−$\mathbf{14}^{4+}$ containing one unpaired electron and were characterized by EPR and UV−vis−near-IR, which showed metal-centered spin and the presence of low-energy IVCT bands. The H_{ab} parameter indicates a relatively strong electronic coupling between the two ruthenium centers (class II). Further two electron oxidation in solution of the $\mathbf{10}^{3+}$−$\mathbf{14}^{3+}$ led to the formation of EPR silent $Ru_2^{III,III}$ complexes $\mathbf{10}^{5+}$−$\mathbf{14}^{5+}$, that were further characterized by UV−vis−NIR. TD-DFT calculations are employed to assign the nature of the UV−vis transitions for the complexes in the various oxidation states, which are of metal to ligand charge transfer (MLCT) type for $Ru_2^{II,II}$ and ligand to metal charge transfer (LMCT) type for $Ru_2^{III,II}$ and $Ru_2^{III,III}$.

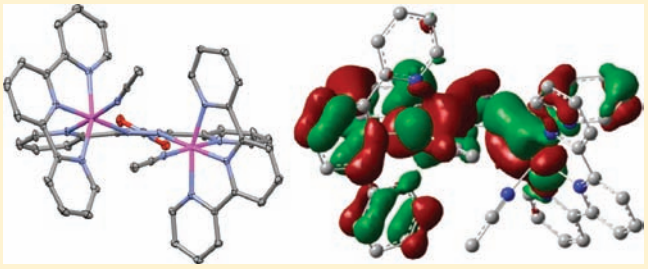

INTRODUCTION

Dinuclear transition metal complexes are of interest because under favorable circumstances the two metal centers can electronically communicate to one another through bridging ligands at long metal−metal distances and thus generate complexes whose natures are radically different from those of the parent mononuclear complexes.[1,2] The interaction of the bridging ligand orbitals with those of the metal centers is one key factor that determines the degree of electronic coupling between the metal centers and is thus in part responsible for the final properties of the complex. In addition, the auxiliary *non*-bridging ligands bonded to the metal center can influence the relative energies of individual metal-based orbitals and therefore these ligands also indirectly influence the electronic communication between the two metal centers.[3] Consequently, for a particular transition metal, a vast array of complexes can be envisaged for which electronic properties can be fine-tuned via the bridging ligand, the auxiliary ligands, or both. This fine-tuning of the electronic interaction is of paramount importance to control magnetic effects[4] and to tune electronic state energies in systems whose reactivities are initiated by means of photochemical and/or redox reactions, including charge separation devices[5] for photochemical solar energy conversion,[6−13] information storage devices,[14−16] and redox catalysis.[17−19]

In the final instance, the catalytic oxidation of water to dioxygen by dinuclear metal complexes,[20] is of particular interest because it constitutes a cornerstone for the design of new energy conversion schemes based on water splitting by sunlight. In this case, reliance upon electron shuttling between the metal centers through the bridging ligand, in order to achieve the overall $4H^+/4e^-$ transfer to generate dioxygen from water, makes the electronic communication between the metal centers the key element in the design of efficient water oxidation catalysts.

So as better to understand the degree of coupling between the two ruthenium centers in the Ru−Hbpp water oxidation catalysts that we have recently described[20−22] and the effect of electronic perturbation both in the bridging and the auxiliary ligands, we have prepared, isolated, and thoroughly characterized a family of structurally related dinuclear RuN_6

Received: August 3, 2011
Published: December 20, 2011

complexes. These complexes have the general formula $\{[Ru^{II}(R^2\text{-trpy})(MeCN)]_2(\mu\text{-}R^1\text{-bpp})\}^{3+}$, $\mathbf{10}^{3+}$–$\mathbf{14}^{3+}$, where R^1-bpp indicates a deprotonated Hbpp ligand substituted at the pyrazolyl ring, and R^2-trpy indicates a trpy ligand substituted at the central pyridyl ring as indicated in Chart 1

Chart 1

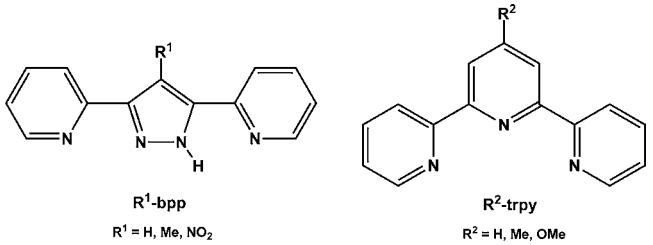

and Scheme 1. In this manner, electronic perturbation is effected through the introduction of electron donating and electron withdrawing substituents in the bridging (bpp) and the auxiliary (trpy) ligands. We have also generated and characterized the corresponding one electron oxidized mixed valence species, $\mathbf{10}^{4+}$–$\mathbf{14}^{4+}$, as well as the subsequent two-electron oxidized species $\mathbf{10}^{5+}$–$\mathbf{14}^{5+}$. We present a thorough characterization of all of these complexes based on spectroscopy (ultraviolet/visible (UV–vis), near-infrared (NIR), electron paramagnetic resonance (EPR)), electrochemistry (cyclic voltammetry (CV), coulometry), and time-dependent density functional theory (TD-DFT).

RESULTS AND DISCUSSION

Synthesis, Structure and Dynamic Behavior. The synthetic strategy employed to prepare the dinuclear RuN_6 complexes $\mathbf{10}^{3+}$–$\mathbf{14}^{3+}$ is depicted in Scheme 1, which also indicates the nomenclature used here. Corresponding new Cl- ($\mathbf{0}^{2+}$–$\mathbf{4}^{2+}$) and OAc-bridged ($\mathbf{5}^{2+}$–$\mathbf{9}^{2+}$) dinuclear complexes were prepared in a manner analogous to those described previously[21] and were used as starting materials to obtain the corresponding MeCN complexes $\{[Ru^{II}(R^2\text{-trpy})(MeCN)]_2(\mu\text{-}R^1\text{-bpp})\}^{3+}$, $\mathbf{10}^{3+}$–$\mathbf{14}^{3+}$, in each case in nearly quantitative yield. These complexes were characterized in the solid state at 100 K by single-crystal X-ray diffraction analysis, Figure 1, and in solution by nuclear magnetic resonance (NMR) spectroscopy (see Supporting Information). In their solid state structures, the Ru centers adopt an octahedral type of coordination and the MeCN monodentate ligands are placed above and below the equatorial plane defined by the nitrogen atoms of the bpp pyrazolate and the central trpy ring. Depending on the relative disposition of these two MeCN ligands, two enantiomeric atropisomers are possible: the ***P*** and ***M*** forms that are found in the unit cell of the crystal structure. However, in solution at room temperature, these atropisomers rapidly interconvert,[23]

$$P \rightarrow M \quad \Delta G^{*} \sim 10\,\text{kcal/mol} \tag{1}$$

with activation free energies in the 10 kcal/mol range as determined from variable-temperature (VT) NMR (see Supporting Information). The electronic perturbations exerted by electron donating or electron withdrawing ligands do not significantly modify the rate of interconversion.

Redox Properties and EPR Spectroscopy. The redox properties of the complexes $\mathbf{10}^{3+}$–$\mathbf{14}^{3+}$, generically labeled as

Scheme 1

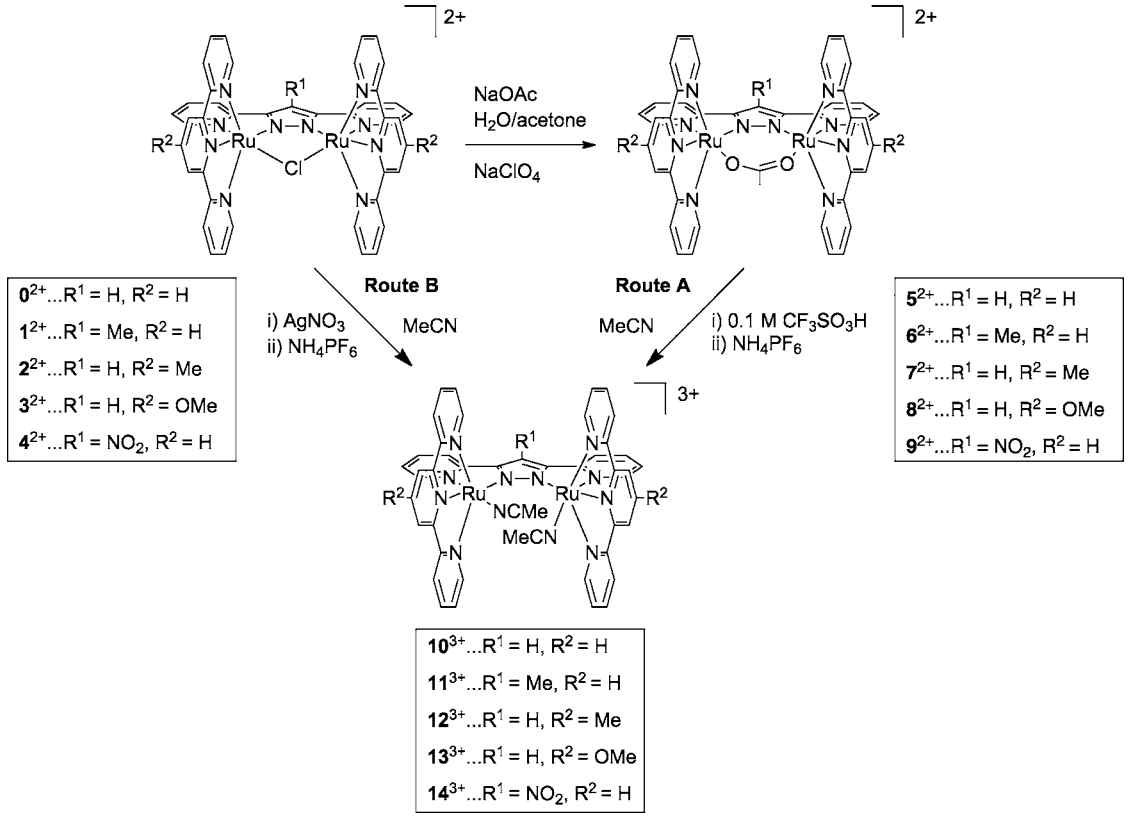

dx.doi.org/10.1021/ic201668r | Inorg. Chem. 2012, 51, 320–327

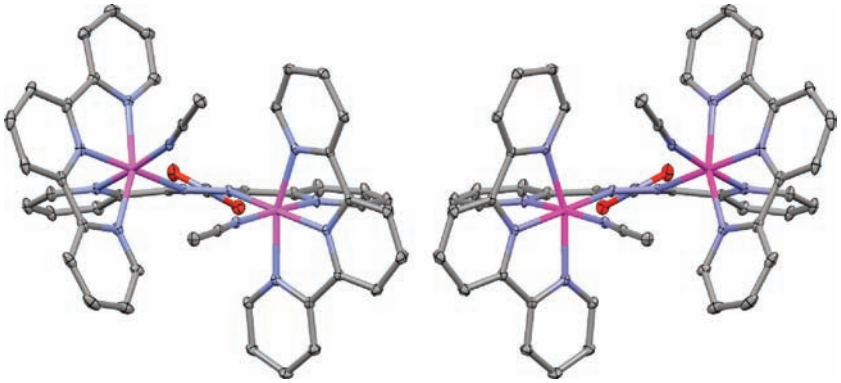

Figure 1. ORTEP plot (ellipsoids at 30% probability) of the molecular structure of the cationic moiety of enantiomeric complexes $\mathbf{14}^{3+}$. Left, *P*-$\mathbf{14}^{3+}$; right, *M*-$\mathbf{14}^{3+}$. Hydrogen atoms are omitted for clarity.

$Ru_2^{II,II}$, were investigated by CV as depicted in Figure 2 (also see Supporting Information) and coulometry, and the most

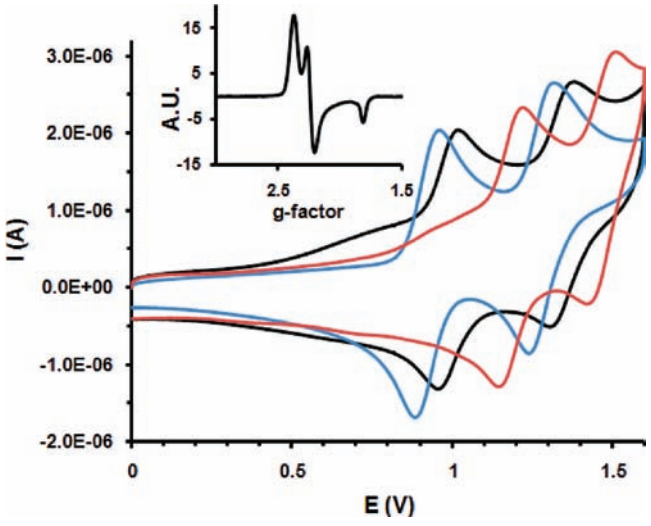

Figure 2. Cyclic voltammograms of complex $\mathbf{10}^{3+}$ (black line). $\mathbf{13}^{3+}$ (blue line) and $\mathbf{14}^{3+}$ (red line) recorded in DCM-TBAH (0.1 M) vs SSCE at 100 mV/s scan rate. Inset, EPR of mixed valence complex $\mathbf{13}^{4+}$.

relevant electrochemical data are gathered in Table 1. The MeCN complexes display two chemically reversible and electrochemically quasireversible electron-transfer (ET) processes. The first process is assigned to the generation of the $Ru_2^{II,III}$ species, $\mathbf{10}^{4+}$–$\mathbf{14}^{4+}$, and the second to the formation of the $Ru_2^{III,III}$ species, $\mathbf{10}^{5+}$–$\mathbf{14}^{5+}$. As expected, the presence of electron donating groups decreases measured reduction potentials, whereas the presence of electron withdrawing groups increases them. Comparing the competing extreme cases of the MeO-substituted complex $\mathbf{13}^{3+}$ and the NO_2-substituted complex $\mathbf{14}^{3+}$, the first redox couple, III,II + $1e^- \rightarrow$ II,II, varies by 255 mV, whereas the second couple, III,III + $1e^- \rightarrow$ III,II, varies by 160 mV. The difference between the two couples, $\Delta E_{1/2} = E_{1/2}^{III,III/III,II} - E_{1/2}^{III,II/II,II}$, ranges from 285 to 380 mV which indicates a relatively strong electronic coupling between the Ru centers. Further, these data permit K_C for the comproportion reaction, $Ru_2^{III,III} + Ru_2^{II,II} \rightarrow 2\ Ru_2^{II,III}$, to be computed, and it ranges from 6.5×10^4 to 2.6×10^6. A general trend that emerges from the data in Table 1 is that electron donating groups increase $\Delta E_{1/2}$, whereas electron withdrawing groups decrease it, except for the case of $\mathbf{12}^{3+}$, where the substitutional difference of H vs Me affects only the individual $E_{1/2}$ values and not the separation between them.

EPR spectroscopy was examined for complexes $\mathbf{10}^{3+}$–$\mathbf{14}^{3+}$ and for their one- and two-electron oxidized species. The $Ru_2^{II,II}$ (low spin d^6–d^6) complexes are diamagnetic, the mixed-valence species $Ru_2^{II,III}$ (d^6–d^5) have one unpaired electron, and the doubly oxidized $Ru_2^{III,III}$ (d^5–d^5) complexes were also found to be EPR silent, manifesting a strong coupling of the locally high-spin Ru centers through the pyrazolate group of the R^1–bpp^- ligand. The mixed valence $Ru_2^{II,III}$ complexes show a rhombic signal that is depicted in the inset of Figure 2; the *g* values obtained for $\mathbf{10}^{4+}$–$\mathbf{14}^{4+}$are provided in the Supporting Information; they are typical for ruthenium-centered spin[24] with only small contributions from the ligands.

UV–Vis Spectroscopy and TD-DFT. Complexes $\mathbf{10}^{3+}$–$\mathbf{14}^{3+}$ and their corresponding one-, $\mathbf{10}^{4+}$–$\mathbf{14}^{4+}$, and two-electron, $\mathbf{10}^{5+}$–$\mathbf{14}^{5+}$, oxidized species were analyzed by means of UV–vis and NIR spectroscopy and by TD-DFT. The most salient spectral details are gathered in Tables 1, 2, and 3; various UV–vis and NIR spectra are provided in Figures 3 and 4 and in the Supporting Information.

Table 1. Electrochemical Data for Complexes $\mathbf{10}^{3+}$–$\mathbf{14}^{3+}$ and Spectroscopic Features of IVCT Bands for the Mixed Valence Complexes $\mathbf{10}^{4+}$–$\mathbf{14}^{4+}$

complex	$E_{1/2}^{III,II/II,II}$ (V) (ΔE, mV)[a]	$E_{1/2}^{III,III/III,II}$ (V) (ΔE, mV)	$\Delta E_{1/2}$ (mV)[b]	K_c	$E_{op} = \nu_{max}$ (cm^{-1})	$\Delta\nu_{1/2}$ (cm^{-1})	$\Delta\nu_{1/2,calc}$ (cm^{-1})[c]	ε ($M^{-1}\cdot cm^{-1}$)	α^2 (cm^{-2})	H_{ab} (cm^{-1})
$\mathbf{10}^{4+}$	0.990 (60)	1.350 (60)	360	1.2×10^6	6250	4080	3800	740	0.010	640
$\mathbf{11}^{4+}$	0.935 (70)	1.325 (90)	390	3.8×10^6	6350	4320	3760	650	0.010	620
$\mathbf{12}^{4+}$	0.950 (60)	1,310 (60)	360	1.2×10^6	6180	4280	3780	785	0.012	670
$\mathbf{13}^{4+}$	0.925 (70)	1.305 (80)	380	2.6×10^6	6110	4480	3830	860	0.014	710
$\mathbf{14}^{4+}$	1.180 (60)	1.465 (70)	285	6.5×10^4	5600	3780	3600	550	0.008	500

[a] $\Delta E = E_{p,c} - E_{p,a}$. [b] $\Delta E_{1/2} = E_{1/2}^{III,III/III,II} - E_{1/2}^{III,II/II,II}$. [c] Calculated with the Hush approximation, $\Delta\nu_{1/2} = (16RT\ln 2(\nu_{max}))^{1/2}$.

dx.doi.org/10.1021/ic201668r | *Inorg. Chem.* 2012, 51, 320–327

Table 2. UV−Vis Spectroscopic Features for Complexes 10^{n+}−14^{n+} (n = 3, 4 and 5) recorded in MeCN-TBAH (0.1 M)

complex (oxidation state)	assig.	λ_{max} (nm) (ε ($M^{-1}cm^{-1}$))
$\mathbf{10}^{3+}$ ($Ru_2^{II,II}$)	$\pi \rightarrow \pi^*$	271 (60300), 310 (71200), 358 (27000)
	$d\pi \rightarrow \pi^*$	445 (13600), 473 (12300), 536 (3100), 615 (800)
$\mathbf{10}^{4+}$ ($Ru_2^{II,III}$)[a]	$d\pi \rightarrow \pi^*$	448 (10000), 630 (6000)
$\mathbf{10}^{5+}$ ($Ru_2^{III,III}$)[a]	$d\pi \rightarrow \pi^*$	417 (7000), 590 (9600)
$\mathbf{11}^{3+}$ ($Ru_2^{II,II}$)	$\pi \rightarrow \pi^*$	271 (57900), 310 (70300), 360 (25200)
	$d\pi \rightarrow \pi^*$	445 (13500), 467 (12100), 532 (3100), 608 (100)
$\mathbf{11}^{4+}$ ($Ru_2^{II,III}$)[a]	$d\pi \rightarrow \pi^*$	453 (8400), 647 (6100)
$\mathbf{11}^{5+}$ ($Ru_2^{III,III}$)[a]	$d\pi \rightarrow \pi^*$	607 (8700)
$\mathbf{12}^{3+}$ ($Ru_2^{II,II}$)	$\pi \rightarrow \pi^*$	271 (59900), 308 (67900), 359 (25300)
	$d\pi \rightarrow \pi^*$	445 (13800), 472 (13000), 533 (3000), 608 (900)
$\mathbf{12}^{4+}$ ($Ru_2^{II,III}$)[a]	$d\pi \rightarrow \pi^*$	447 (9800), 630 (5200)
$\mathbf{12}^{5+}$ ($Ru_2^{III,III}$)[a]	$d\pi \rightarrow \pi^*$	410 (5200), 588 (6400)
$\mathbf{13}^{3+}$ ($Ru_2^{II,II}$)	$\pi \rightarrow \pi^*$	272 (71700), 305 (66600), 360 (28800)
	$d\pi \rightarrow \pi^*$	446 (16300), 474 (15400), 595 (1000)
$\mathbf{13}^{4+}$ ($Ru_2^{II,III}$)[a]	$d\pi \rightarrow \pi^*$	448 (12100), 622 (6400)
$\mathbf{13}^{5+}$ ($Ru_2^{III,III}$)[a]	$d\pi \rightarrow \pi^*$	409 (7600), 581 (10400)
$\mathbf{14}^{3+}$ ($Ru_2^{II,II}$)	$d\pi \rightarrow \pi^*$	440 (13700), 640 (3900), 592 (1800)
$\mathbf{14}^{4+}$ ($Ru_2^{II,III}$)[a]	$d\pi \rightarrow \pi^*$	440 (13700), 640 (3900)
$\mathbf{14}^{5+}$ ($Ru_2^{III,III}$)[a]	$d\pi \rightarrow \pi^*$	420 (7100), 548 (6500)

[a]Oxidation was achieved by controlled bulk electrolysis at specific potential ($E_{appl} \geq E_{1/2}$ + 150 mV) in a 1 mm three electrode spectro-electrochemical cell.

Table 3. Visible Absorption Maxima and Substitution Effects for Complexes 10^{n+}−14^{n+} (n = 3, 4 and 5)

	complex														
	$Ru_2^{II,II}$					$Ru_2^{II,III}$					$Ru_2^{III,III}$				
	$\mathbf{10}^{3+}$	$\mathbf{11}^{3+}$	$\mathbf{12}^{3+}$	$\mathbf{13}^{3+}$	$\mathbf{14}^{3+}$	$\mathbf{10}^{4+}$	$\mathbf{11}^{4+}$	$\mathbf{12}^{4+}$	$\mathbf{13}^{4+}$	$\mathbf{14}^{4+}$	$\mathbf{10}^{5+}$	$\mathbf{11}^{5+}$	$\mathbf{12}^{5+}$	$\mathbf{13}^{5+}$	$\mathbf{14}^{5+}$
λ_{max}(exp)	473	475	472	474	464	630	647	630	622	640	590	607	588	581	548
$\Delta\lambda_{max}$[a] (exp)	–	+2	−1	+1	−9	–	+17	±0	−8	−[b]	–	+17	−2	−9	−42
$\Delta\lambda_{max}$(calc)	–	–	–	–	–	–	+14	−5	−12	−44	–	+23	−8	−23	−46

[a]$\Delta\lambda_{max} = \lambda_{max}(Y^{n+}) - \lambda_{max}(\mathbf{10}^{n+})$ (Y = **11**, **12**, **13**, or **14**; n = 3, 4 or 5). [b]Not assigned as peak cannot be resolved within a shoulder; see Figure 4.

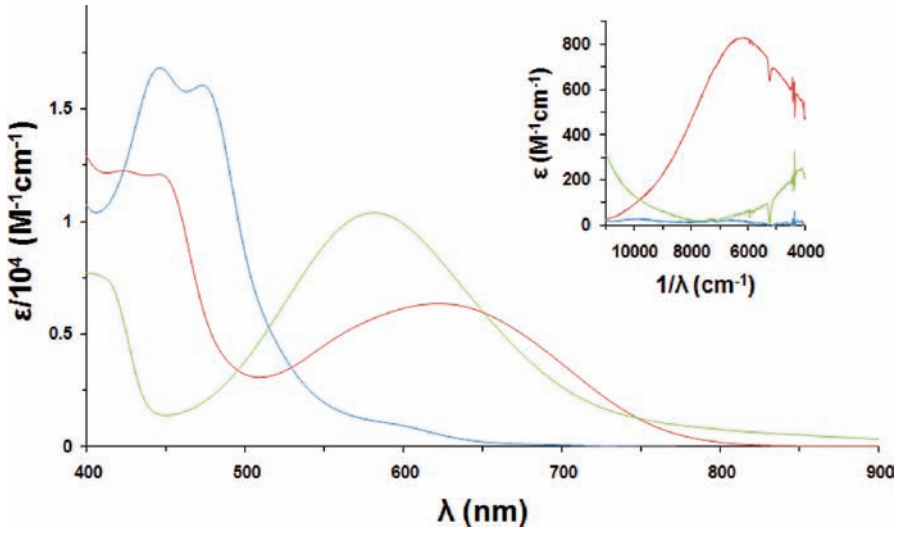

Figure 3. UV−vis and NIR (inset) spectra of $\mathbf{13}^{3+}$ (blue line), $\mathbf{13}^{4+}$ (green line), and $\mathbf{13}^{5+}$ (red line) recorded in MeCN-TBAH (0.1 M).

The UV−vis spectrum of $\mathbf{13}^{3+}$ (Figure 3) shows a set of intense MLCT bands in the range of 400−550 nm and very weak dd bands at around 600 nm, as would be expected for low-spin d^6 $Ru^{II}N_6$ complexes.[25] The one- and two-electron oxidized species $\mathbf{13}^{4+}$ (d^6−d^5) and $\mathbf{13}^{5+}$ (d^5−d^5) show a decrease of intensity and a blue (hypsochromic) shift of their MLCT bands; in addition, for each case, a new, intense band is found in the 550−750 nm region (Figure 3).

UV−vis spectra for the whole series of complexes $\mathbf{10}^{n+}$−$\mathbf{14}^{n+}$ (n = 3, 4, and 5) are provided in the Supporting Information while the visible-region spectra for $\mathbf{10}^{4+}$−$\mathbf{14}^{4+}$ and $\mathbf{10}^{5+}$−$\mathbf{14}^{5+}$ are presented in Figure 4. For the case of the $Ru_2^{II,II}$ (d^6−d^6) complexes, the electronic perturbations exerted by the electron

dx.doi.org/10.1021/ic201668r | Inorg. Chem. 2012, 51, 320−327

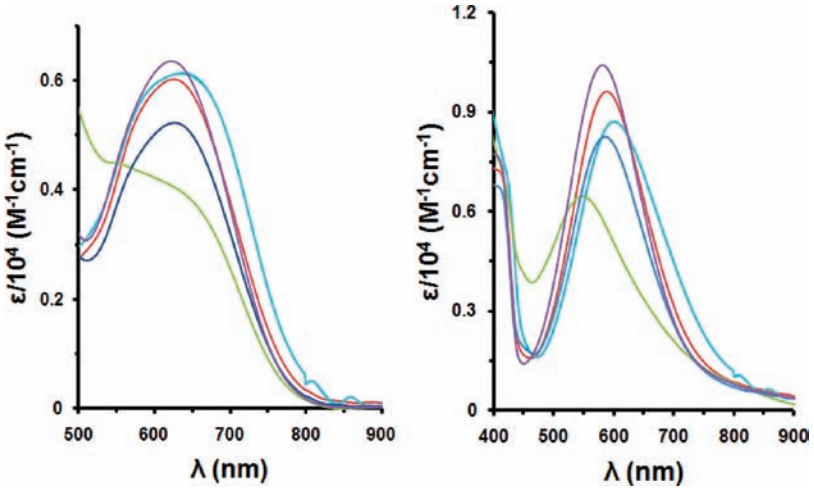

Figure 4. Vis spectra for: left, $Ru_2^{II,III}$ complexes $\mathbf{10}^{4+}$–$\mathbf{14}^{4+}$ and right, $Ru_2^{III,III}$ complexes $\mathbf{10}^{5+}$–$\mathbf{14}^{5+}$. Color code: $\mathbf{10}^{x+}$ (red), $\mathbf{11}^{x+}$ (turquoise), $\mathbf{12}^{x+}$ (blue), $\mathbf{13}^{x+}$ (purple), and $\mathbf{14}^{x+}$ (green).

donating and electron withdrawing groups are almost negligible, while for the $Ru_2^{II,III}$ (d^6–d^5) and $Ru_2^{III,III}$ (d^5–d^5) cases, more distinct trends can be observed. This stands in sharp contrast to the strong influence observed for electron donating and electron withdrawing groups on the redox potentials as described above.

In general, it is known that electron donating groups[25] destabilize the π^*(L) orbitals of the bpp^- and trpy ligands and, to a lesser extent, they also destabilize the remote dπ(Ru) orbitals, whereas the opposite is true for electron withdrawing groups. However, in the present case, there are two factors that can complicate an otherwise easy prediction of MLCT relative energies based on such simple qualitative arguments. One is the relatively similar energies of the trpy and bpp^- π^* orbitals that might dilute the destabilizing effect associated with substitution on only a single ligand, and the second is the potential hybridization, i.e., covalent mixing, of the dπ(Ru) and π(trpy and/or bpp^-) orbitals.

To explore these electronic-structure issues in detail, TD-DFT calculations employing the hybrid B3LYP density functional and accounting for nonequilibrium solvation in acetonitrile were undertaken for the one- and two-electron oxidized complexes, where substitution effects are most evident (details of the computational procedures are provided in Supporting Information). Experimental visible absorption maxima (λ_{max}) and substitution effects relative to $\mathbf{10}^{n+}$ ($\Delta\lambda_{max}$) are provided in Table 3. TD B3LYP $\Delta\lambda_{max}$ values for $\mathbf{10}^{n+}$–$\mathbf{14}^{n+}$ (n = 4,5) are also listed in Table 3. As we are interested primarily in substitution effects, we do not present the absolute TD-B3LYP λ_{max} here, but they may be found in the Supporting Information together with a description of the molecular orbitals involved in the individual excitations; the quantitative accuracy of the λ_{max} values is very good, with all predictions within 0.1 eV of the measured values. Given that level of accuracy for B3LYP, we conclude that there is little merit in assessing the performance of other functionals in this instance.

All of the $\Delta\lambda_{max}$ values predicted at the TD-B3LYP level have the correct sign and are in good quantitative agreement with the available experimental data (the mean unsigned error over seven measurements is 6 nm, noting that in this region of the visible spectrum an error of 1 nm in wavelength corresponds to an energy error of only about 3 meV). Analysis of the TD-B3LYP excitations reveals the visible bands in the one- and two-electron oxidized species to be quite complex in character. Taking $\mathbf{10}^{4+}$ to begin, the TD-B3LYP eigenvector for the relevant absorption indicates three different one-electron excitations to contribute with weights of 0.57, 0.14, and 0.14. All of the excitations take place into the same acceptor orbital, which is the lowest unoccupied molecular orbital (LUMO) in the β manifold (nominally the hole on the oxidized Ru center, with some contribution from a bpp^- π^* orbital), but the individual occupied orbitals from which the excitations occur are diverse and well below the highest occupied molecular orbital (HOMO) in the manifold, as illustrated in Figure 5. While the occupied orbitals *do* exhibit some amplitude on the Ru atoms, it is generally quite small in magnitude compared to the amplitude distributed over ligand atoms (π-type orbitals), so that the transitions in $\mathbf{10}^{4+}$ and its substituted congeners may be properly described as ligand to metal charge transfer (LMCT) in character. As can be observed in Figure 5, the various occupied orbitals are generally mixtures of bpp^- and trpy π orbitals with similar weights, although orbital 235 is reasonably dominated by trpy character.

In the substituted one-electron oxidized species, the substituents play two interrelated roles: to the extent that a substituent adjusts the relative energy of one or more of the occupied orbitals, it also influences the relative weight of that orbital in the TD-B3LYP excitation eigenvector. The interrelationship is complex and leads to instances ranging from all three excitations continuing to have significant contribution ($\mathbf{13}^{4+}$) to a single excitation mostly, but not completely, dominating ($\mathbf{14}^{4+}$; HOMO-9 → LUMO about 72% of total). Rationalizing the precise changes in weight of the contributing excitations is not practical (although the data and orbitals are provided in full in the Supporting Information). However, some qualitative information can be obtained from the orbital analysis. Inspection of Figure 5 indicates that most of the donor orbitals have substantial amplitude on the bpp^- carbon atom that is substituted in compounds $\mathbf{11}^{4+}$ and $\mathbf{14}^{4+}$. On the other hand, two of the three donor orbitals have effectively *zero* amplitude on the trpy carbon atom that is substituted (note that, not surprisingly, it is the trpy on the less oxidized Ru atom that acts as a donor to the more oxidized Ru atom in the excitation). Given this orbital picture, one would expect the LMCT transition to be more sensitive to bpp^--

dx.doi.org/10.1021/ic201668r | *Inorg. Chem.* 2012, 51, 320–327

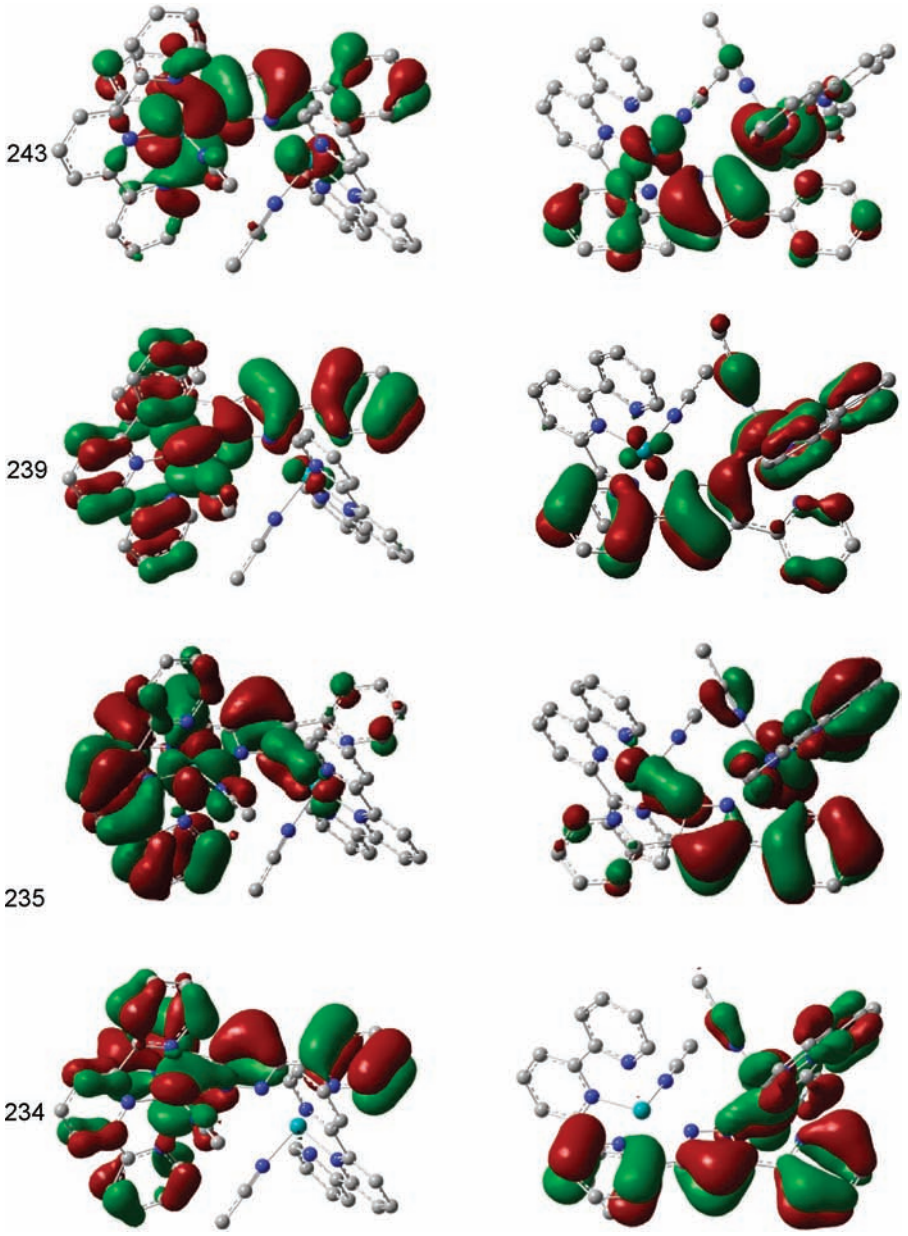

Figure 5. B3LYP orbitals involved in the transition predicted in the visible region for complex $\mathbf{10}^{4+}$. The view on the left places the bpp^- ligand behind the Ru centers and the MeCN ligands in front, tilted somewhat so that the bpp^- ligand is raised and the MeCN ligands lowered; the view on the right reverses this perspective by rotating the complex about an axis orthogonal to the plane of the bpp^- ring. Carbon atoms are gray, nitrogen atoms blue, oxygen atoms red, and Ru atoms cyan; hydrogen atoms are not shown for clarity. The orbitals are numbered according to ground-state energies and correspond (in the β manifold) to HOMO-9, HOMO-8, HOMO-4, and LUMO.

substitution compared to trpy-substitution, and inspection of Table 3 indicates this to be true for the case of a methyl substituent, comparing $\mathbf{11}^{4+}$ to $\mathbf{12}^{4+}$ (it is also true comparing the NO_2-bpp^- case to MeO-trpy, but as the two substituents are different, it is not clear that this comparison should be regarded as definitive).

Considering the role of the electron donating vs electron withdrawing groups, the measured and predicted spectral shifts are paradoxical for the substitutions on the trpy ligand. Given that the nature of the transition is LMCT, one might expect to observe a blue-shift ($\Delta\lambda_{max} < 0$) for electron withdrawing groups and a red-shift ($\Delta\lambda_{max} > 0$) for electron donating groups. However, the opposite trend is observed for MeO, and a Me group on the trpy ligand has essentially no effect. On the other hand, the Me and NO_2 substitutions on the bpp^- ligand yields the expected red- and blue-shifts, respectively. Inspection of the molecular orbitals involved in the substituted-system transitions indicates that the relevant orbitals place very little to no amplitude on the substituents. As such, the influence of the substituents seems to have less to do with their inductive character and more with the degree to which they modify the weights of the different contributions. Indeed, this helps to explain why the total range of excitation energies is actually quite narrow, in spite of the generally strong character of NO_2 and MeO as electron withdrawing and electron donating groups, respectively; the span of 25 nm observed experimentally in this region of the spectrum corresponds to a variation of only 78 meV, or 1.8 kcal/mol.

dx.doi.org/10.1021/ic201668r | *Inorg. Chem.* 2012, 51, 320–327

Considering the TD-B3LYP results for the doubly oxidized systems, the analysis is quite similar, although the precise ordering of the orbitals in the energy manifold is somewhat different than in the singly oxidized case (and, in this antiferromagnetically coupled singlet, α and β excitations have near identical weights, as expected). Again, the span of energetic influence associated with substitution is not particularly large. TD-B3LYP corroborates these observations, which again suggests that a subtle combination of inductive effects and variations in excitation character play a role in modulating substituent influence.

We might expect in a system having ligands of less similar donating character than trpy vs bpp$^-$ we would see more substitution influence as it would be less possible to modulate the character of the excitation. Indeed, we may regard the electrochemical results as some indicator that this would be true. Oxidation involves complete loss of an electron, as opposed to internal electronic redistribution, and it is clear from the CV data that substitution has a much more significant influence on the reduction potentials, and one that is moreover in the intuitively expected direction.

Near-IR Absorption and Electronic Coupling. Of the various oxidation states of **13** considered in this work, only the one-electron oxidized mixed valence complex $\mathbf{13}^{4+}$ has an absorption in the 3000−11000 cm^{-1} NIR zone (inset, Figure 3) that is expected for a typical intervalence charge-transfer (IVCT) band.[26−28] Similar NIR spectra were recorded for all complexes $\mathbf{10}^{4+}$−$\mathbf{14}^{4+}$ and are reported in Figure 3 and in the Supporting Information In a symmetric system ($\Delta G = 0$) and thus following the Franck−Condon principle, the energy of the IVCT transition $E_{op} = \lambda$, the absorption wavelength expressed in energy units. From the spectra, the delocalization parameter, α^2, and the electronic coupling constant, H_{ab}, can be calculated using eqs 2 and 3 respectively:[3,28]

$$\alpha^2 = ((4.2 \times 10^{-4})\varepsilon_{max}\Delta\nu_{1/2})/d^2E_{op} \quad (2)$$

$$H_{ab} = (\alpha^2 E_{op}{}^2)^{1/2} \quad (3)$$

where ε_{max} is the extinction coefficient of λ_{max} of the IVCT band and "d" is the metal−metal distance in Å. These spectral parameters have been calculated for all complexes and are displayed in Table 1. As can be observed from Table 1, these complexes can be considered class II ($0 < H_{ab} < \lambda/2$) according to Robin-Day, where intermediate electronic coupling among the metal centers is observed in agreement with previous related complexes.[3,26] Further support for class II is given by the good agreement between the calculated $\Delta\nu_{1/2}$ values using the Hush formalism and the experimental one.

As can be observed in Table 1, complexes containing electron donating groups enhance the electronic coupling constant, H_{ab}, between the Ru centers whereas electron withdrawing groups decrease it, except for the case of $\mathbf{11}^{4+}$. This is in agreement with the trends observed for the $\Delta E_{1/2}$ values in the redox section.

CONCLUSIONS

We have prepared a family of dinuclear RuN_6 type of complexes of general formula $\{[Ru^{II}(R^2\text{-trpy})(MeCN)]_2(\mu\text{-}R^1\text{-bpp})\}^{3+}$, $\mathbf{10}^{3+}$−$\mathbf{14}^{3+}$, that are structural analogues of the Ru−Hbpp water oxidation catalyst where the aqua groups have been substituted by MeCN ligands. In these complexes, electronic perturbations are exerted via electron donating and electron withdrawing substituents both at the trpy and bpp$^-$ ligands. CV experiments indicate that those electron donating and electron withdrawing groups strongly affect their corresponding $E_o^{III,III-III,II}$ and $E_o^{III,II-II,II}$ potentials but their EPR and UV−vis spectroscopic features are relatively unaffected. TD-DFT calculations rationalize the LMCT nature of the visible bands for the $Ru_2^{III,II}$ and $Ru_2^{III,III}$ complexes and suggest that their relative insensitivity to substitution derives from the involvement of several donor orbitals distributed over both the bpp$^-$ and trpy ligands in the relevant excitation. Near-IR spectroscopy for the mixed valence species $Ru_2^{III,II}$ allows calculation of the H_{ab} parameter that indicates a relatively strong electronic coupling (class II) between the two ruthenium centers through the pyrazolyl ring of the bpp$^-$ ligand. This is in agreement with the large K_c values derived from electrochemical measurements and from EPR silent nature of the $Ru_2^{III,III}$ species. Finally, electron donating groups in general produce an enhancement of the electronic coupling whereas electron withdrawing groups produce the opposite effect. A significant result of this work, in connection with the dinuclear water oxidation catalysts, is that electron donating groups enhance the electronic communication between the metal centers and thus can improve the electron transfer (ET) kinetics between them which will in turn render these complexes as more efficient water oxidation catalysts.

ASSOCIATED CONTENT

Supporting Information

Experimental section, X-ray structures, NMR, UV−vis-NIR, EPR, Echem, references. Theoretical calculations: computational methods, DFT, calcd HOMOs and LUMOs and energies, references. Crystallographic information (CIF). This material is available free of charge via the Internet at http://pubs.acs.org.

AUTHOR INFORMATION

Corresponding Author

*E-mail: cramer@umn.edu (C.J.C.), allobet@iciq.es (A.Ll.).

ACKNOWLEDGMENTS

Support from SOLAR-H2 (EU 212508) and MICINN (CTQ2010−21497; Consolider Ingenio 2010 (CSD2006−0003)), and the U.S. National Science Foundation (CHE09-52054) are gratefully acknowledged. S.R. is grateful for the award of a doctoral grant also from MICINN.

REFERENCES

(1) Aguirre-Etcheverry, P.; O'Hare, D. *Chem. Rev.* **2010**, *110*, 4839−4864.
(2) York, J. T.; Llobet, A.; Cramer, C. J.; Tolman, W. B. *J. Am. Chem. Soc.* **2007**, *129*, 7990−7999.
(3) Browne, W. R.; Hage, R.; Vos, J. G. *Coord. Chem. Rev.* **2006**, *250*, 1653−1668.
(4) Carlson, C. N.; Veauthier, J. M.; John, K. D.; Morris, D. E. *Chem.—Eur. J.* **2008**, *14*, 422−431.
(5) Matsumoto, M. Y.; Toyama, M. M.; Mayer, I.; Winnischofer, H.; Araki, K.; Toma, H. E. *J. Braz. Chem. Soc.* **2009**, *20*, 728−736.
(6) Kalyanasundaram, K. *Coord. Chem. Rev.* **1982**, *46*, 159−244.
(7) Lehn, J.-M. *Angew. Chem., Int. Ed.* **1988**, *27*, 89−112.
(8) Balzani, V.; Campagna, S.; Denti, G.; Juris, A.; Serroni, S.; Venturi, M. *Coord. Chem. Rev.* **1994**, *132*, 1−13.
(9) Balzani, V.; Juris, A.; Venturi, M.; Campagna, S.; Serroni, S. *Chem. Rev.* **1996**, *96*, 759−834.

(10) Balzani, V.; Campagna, S.; Denti, G.; Juris, A.; Serroni, S.; Venturi, M. *Acc. Chem. Res.* **1998**, *31*, 26−34.
(11) Slate, C. A.; Striplin, D. R.; Moss, J. A.; Chen, P.; Erickson, B. W.; Meyer, T. J. *J. Am. Chem. Soc.* **1998**, *120*, 4885−4886.
(12) Hu, Y.-Z.; Tsukiji, S.; Shinkai, S.; Oishi, S.; Hamachi, I. *J. Am. Chem. Soc.* **1999**, *122*, 241−253.
(13) Sauvage, J. P.; Collin, J. P.; Chambron, J. C.; Guillerez, S.; Coudret, C.; Balzani, V.; Barigelletti, F.; De Cola, L.; Flamigni, L. *Chem. Rev.* **1994**, *94*, 993−1019.
(14) Balzani, V.; Scandola, F., *Supramolecular Photochemistry*; Ellis Horwood Ltd.: Chichester, UK, 1991.
(15) Balzani, V., *Supramolecular Photochemistry*; Springer: Dordrecht, 1987.
(16) Lehn, J.-M., *Supramolecular Chemistry*; Wiley-VCH: Weinheim, 1995.
(17) Gilbert, J. A.; Eggleston, D. S.; Murphy, W. R.; Geselowitz, D. A.; Gersten, S. W.; Hodgson, D. J.; Meyer, T. J. *J. Am. Chem. Soc.* **1985**, *107*, 3855−3864.
(18) Wasylenko, D. J.; Ganesamoorthy, C.; Henderson, M. A.; Koivisto, B. D.; Osthoff, H. D.; Berlinguette, C. P. *J. Am. Chem. Soc.* **2010**, *132*, 16094−16106.
(19) Wasylenko, D. J.; Ganesamoorthy, C.; Koivisto, B. D.; Henderson, M. A.; Berlinguette, C. P. *Inorg. Chem.* **2010**, *49*, 2202−2209.
(20) Sala, X.; Romero, I.; Rodríguez, M.; Escriche, L.; Llobet, A. *Angew. Chem., Int. Ed.* **2009**, *48*, 2842−2852.
(21) Sens, C.; Romero, I.; Rodríguez, M.; Llobet, A.; Parella, T.; Benet-Buchholz, J. *J. Am. Chem. Soc.* **2004**, *126*, 7798−7799.
(22) Bozoglian, F.; Romain, S.; Ertem, M. Z.; Todorova, T. K.; Sens, C.; Mola, J.; Rodriguez, M.; Romero, I.; Benet-Buchholz, J.; Fontrodona, X.; Cramer, C. J.; Gagliardi, L.; Llobet, A. *J. Am. Chem. Soc.* **2009**, *131*, 15176−15187.
(23) Planas, N.; Christian, G.; Mas-Marzá, E.; Sala, X.; Fontrodona, X.; Maseras, F.; Llobet, A. *Chem.—Eur. J.* **2010**, *16*, 7965−7968.
(24) Patra, S.; Sarkar, B.; Mobin, S. M.; Kaim, W.; Lahiri, G. K. *Inorg. Chem.* **2003**, *42*, 6469−6473.
(25) Bargawi, K. R.; Llobet, A.; Meyer, T. J. *J. Am. Chem. Soc.* **1988**, *110*, 7751−7759.
(26) Baitalik, S.; Florke, U.; Nag, K. *J. Chem. Soc., Dalton Trans.* **1999**, 719−728.
(27) D'Alessandro, D. M.; Keene, F. R. *Chem. Soc. Rev.* **2006**, *35*, 424−440.
(28) D'Alessandro, D. M.; Keene, F. R. *Chem.—Eur. J.* **2005**, *11*, 3679−3688.